Physics and Imaging in Radiation Oncology 33 (2025) 100688

Contents lists available at ScienceDirect

Physics and Imaging in Radiation Oncology

journal homepage: www.sciencedirect.com/journal/physics-and-imaging-in-radiation-oncology

Original research article

Investigating the potential of diffusion tensor atlases to generate anisotropic clinical tumor volumes in glioblastoma patients

Kim Hochreuter [a,b], Gregory Buti [d], Ali Ajdari [d], Christopher P. Bridge [e], Gregory C. Sharp [d], Sune Jespersen [f,g], Slávka Lukacova [b,c], Thomas Bortfeld [d], Jesper F. Kallehauge [a,b,*]

[a] Aarhus University Hospital, Danish Centre for Particle Therapy, Palle Juul-Jensens Blvd. 25, 8200 Aarhus, Denmark
[b] Aarhus University, Department of Clinical Medicine, Palle Juul-Jensens Blvd. 82, 8200 Aarhus, Denmark
[c] Aarhus University Hospital, Department of Oncology, Palle Juul-Jensens Blvd. 99, 8200 Aarhus, Denmark
[d] Massachusetts General Hospital and Harvard Medical School, Department of Radiation Oncology, Division of Radiation Biophysics, 100 Blossom St, Boston, MA 02114, USA
[e] Massachusetts General Hospital and Harvard Medical School, Athinoula A. Martinos Center for Biomedical Imaging, 149 Thirteenth St, Charlestown, MA 02129, USA
[f] Center of Functionally Integrative Neuroscience, Department of Clinical Medicine, Aarhus University, Aarhus, Denmark
[g] Department of Physics and Astronomy, Aarhus University, Aarhus, Denmark

ARTICLE INFO

Keywords:
Radiotherapy
CTV
DTI
Anisotropic margin expansion
Glioblastoma

ABSTRACT

Background and purpose: Diffusion tensor imaging (DTI) has been proposed to guide the anisotropic expansion from gross tumor volume to clinical target volume (CTV), aiming to integrate known tumor spread patterns into the CTV. This study investigate the potential of using a DTI atlas as an alternative to patient-specific DTI for generating anisotropic CTVs.

Materials and Methods: The dataset consisted of twenty-eight newly diagnosed glioblastoma patients from a Danish national DTI protocol with post-operative T1-contrast and DTI imaging. Three different DTI atlases, spatially aligned to the patient images using deformable image registration, were considered as alternatives. Anisotropic CTVs were constructed to match the volume of a 15 mm isotropic expansion by generating 3D distance maps using either patient- or atlas-DTI as input to the shortest path solver. The degree of CTV anisotropy was controlled by the migration ratio, modeling tumor cell migration along the dominant white matter fiber direction extracted from DTI. The similarity between patient- and atlas-DTI CTVs was analyzed using the Dice Similarity Coefficient (DSC), with significance testing according to a Wilcoxon test.

Results: The median (range) DSC between anisotropic CTVs generated using patient-specific and atlas-based DTI was 0.96 (0.93–0.97), 0.96 (0.93–0.97), and 0.95 (0.93–0.97) for the three atlases, respectively ($p > 0.01$), for a migration ratio of 10. The results remained consistent over the range of studied migration ratios (2 to 100).

Conclusion: The high degree of similarity between all anisotropic CTVs indicates that atlas-DTI is a viable replacement for patient-specific DTI for incorporating fiber direction into the CTV.

1. Introduction

Glioblastomas (GBMs) are aggressive and infiltrative brain tumors with a poor prognosis. The current standard treatment for GBMs is a combination of surgery, chemo-radiation and adjuvant chemotherapy [1]. Radiotherapy is used to treat both the detectable tumor, i.e. Gross Tumor Volume (GTV), as well as the surrounding microscopic tumor spread which is not visible on medical images. To account for microscopic spread, the Clinical Target Volume (CTV) is defined in treatment planning by adding a safety margin to the GTV. According to the ESTRO-EANO guidelines, the CTV is defined as a 1.5 cm isotropic expansion around the GTV [2], which is then corrected for anatomical barriers such as the falx cerebri, ventricles, and skull.

Correlations have been found between the extent of tumor presence in the white matter and imaging data, suggesting that tumor cells preferentially migrate along axonal tracts in the white matter [3–5]. Such spread patterns may not be adequately captured by an isotropic

* Correspondence to: Danish Centre for Particle Therapy, Aarhus University Hospital, Aarhus, Denmark.
E-mail address: jespkall@rm.dk (J.F. Kallehauge).

https://doi.org/10.1016/j.phro.2024.100688
Received 16 July 2024; Received in revised form 5 December 2024; Accepted 10 December 2024
Available online 24 December 2024

GTV-to-CTV expansion [6,7]. Therefore, incorporating patient-specific anatomical and microstructural information may be an important step in personalizing and ultimately improving the definition of the CTV.

Diffusion Weighted Imaging (DWI) is a technique used to probe microstructural information of tissue, most commonly in the brain. DWI is based on the acquisition of magnetic resonance imaging (MRI) sequences that can measure the diffusion of water molecules in tissues without the need for exogenous chemical agents. Diffusion Tensor Imaging (DTI) is an extension of DWI and is used to estimate the degree of anisotropy and orientation in tissue. The most popular application of DTI is the structural mapping of tissues at the cellular level in the brain. In particular, the structure of axon fibers connecting neurons in the brain is of interest. The method of DTI has been used in clinical research to study the effect of aging, multiple sclerosis and epilepsy on axon fibers [8–10].

The diffusion patterns of water molecules provided by DTI serve as a roadmap used to model preferential migration of GBM inside white matter. Using DTI to design anisotropic CTVs has been attempted for nearly a decade [11–15]. However, given the small cohorts and lack of prospective studies, it is still an open question whether a DTI-based CTV definition is clinically feasible.

An alternative to adding a DTI sequence for each patient (patient-DTI) as part of the radiotherapy treatment planning scans is to use a DTI atlas (atlas-DTI), by spatially matching the atlas to each patient. Such an approach approximates the diffusion patterns of water in each individual patient. However, the main concern with using an atlas-DTI is that it is unclear if it can reproduce tumor-induced and surgical effects since it was developed using a healthy cohort. The methodology to incorporate an atlas-DTI to generate CTVs has been proposed in Buti et al., but validation against a ground truth was missing [16]. Stretton et al. showed that atlas-DTI can adequately reproduce tumor spread compared to patient-DTI [17]. However, the analysis was performed on a small cohort of three patients, which may not be representative of the heterogeneity in the patient population.

The aim of this study was to evaluate the accuracy of an atlas-DTI as a surrogate to patient-DTI for generation of anisotropic CTV expansions. The analysis include CTV generation with different choices of model parameters, e.g., tumor migration in white matter over gray matter. Finally, the clinical implications of the choice of model-based anisotropic CTVs over manually-edited isotropic CTVs will be presented and discussed.

2. Methods

First, an overview is given of the patient and imaging data used in the study. Second, the workflow is presented for generating anisotropic CTVs using patient- and atlas-DTI. Third, the evaluation metrics and data pre-processing procedures are described.

2.1. Patient data

This study used data from a Danish national DTI protocol, approved by the Central Denmark Region Committees on Health Research Ethics (Reg. no. 1-10-72-184-21). All participating patients provided written informed consent. This protocol is a non-interventional prospective trial, in which DWI scans were conducted as part of the imaging protocol for radiotherapy treatment planning (referred to as therapy scans).

Twenty-eight patients were selected. All patients were adults with newly diagnosed and pathology confirmed glioblastoma IDH wildtype, according to WHO 2021 classification [18], ECOG performance status of 0 or 1 and referred for long-course radio-chemotherapy. Patient characteristics are presented in Supplementary Table 1.

From the post-operative therapy scans, the contrast-enhanced T1-weighted image (T1C), DWI (Philips Ingenia 3T), and Computed Tomography (CT, Siemens Somatom Definition Edge) were used. Additionally, the GTV, CTV, and brain mask were acquired. All DWI were derived using a diffusion weighting of $b = 0, 1000$ s/mm^2 in 32 directions. Prior to estimation of the DTI, the DWI underwent extensive pre-processing steps to reduce artifacts and noise, as suggested in [19,20].

Three atlas-DTI were investigated as potential surrogates for a patient-DTI: HCP1065 [21], IIT [22] and MIITRA [23]. The atlases differ in their size and age range of the cohorts. The cohort size was 1065, 72, and 202 subjects, and the age range was 22–37, 20–39, and 65–95 for the HCP, IIT, and MIITRA atlases, respectively.

In order to use the atlas-DTIs in the patient-specific setting, an image registration step was performed to spatially align the atlas-DTIs to the patient images. We used the brain image registration software *Advanced Normalization Tools* (ANTs) [24]. First, the atlas T1-weighted (T1) image associated with the atlas-DTI was registered to the patient T1C image using a deformable image registration (DIR) process. ANTs then applies the displacement vector field to the atlas-DTI using a tensor transformation model called the preservation of principal direction (PPD) [25].

2.2. Geometric expansion model to generate the CTV

We followed the methodology proposed in Refs. [16,26] to generate the CTV for each patient. The CTV is defined as an iso-distance contour in a 3D distance map with the GTV at the origin. The distance at each point $r = (x, y, z)$ is obtained solving the shortest-path problem:

$$\nabla^{\mathsf{T}} S(r)\mathcal{G}(r)^{-1}\nabla S(r) = 1, \tag{1}$$

where ∇ is the gradient operator, T the transpose, and $\mathcal{G}^{-1}$ is the inverse of a second order tensor $\mathcal{G}$, called the Riemannian *metric tensor*. $\mathcal{G}(r)$ is the entity that integrates preferential pathways of tumor spread and anatomical barriers.

Preferential pathways were derived from the DTI. Let D denote the patient- or atlas DTI tensors at point r in the image. D can be reformulated using spectral decomposition [27]:

$$D(r) = Q(r)\Lambda(r)Q(r)^{-1}, \tag{2}$$

with the eigenvector matrix $Q = (\mathbf{q}_1, \mathbf{q}_2, \mathbf{q}_3)$ and the corresponding eigenvalue matrix $\Lambda = \mathrm{diag}(\lambda_1, \lambda_2, \lambda_3)$. The eigenvectors were sorted as $\lambda_1 \geq \lambda_2 \geq \lambda_3$ so that $\mathbf{q}_1$ is the dominant diffusion direction. White matter voxels typically have a strong directionality $\lambda_1 \gg \lambda_2 \geq \lambda_3 \geq 0$, while the voxels in gray matter and cerebrospinal fluid have approximately equal eigenvalues.

$\mathcal{G}$ and D are inversely related to each other [26]. Therefore, $\mathcal{G}$ can be constructed in a piecewise fashion by using the DTI eigenvectors in white matter but replacing the DTI eigenvalues by the parameterized matrix $(\sigma, 1, 1)$, and setting the gray matter and barrier structures to unity and zero:

$$\mathcal{G}(r)^{-1} = \begin{cases} Q(r)\mathrm{diag}(\sigma, 1, 1)Q(r)^{-1} & \forall r \in \text{white matter}, \\ \mathbb{I}_3 & \forall r \in \text{gray matter}, \\ \mathbb{O}_3 & \forall r \in \text{barriers}, \end{cases} \tag{3}$$

with $\mathbb{I}_3$ the 3×3 identity matrix and $\mathbb{O}_3$ the 3×3 zero matrix. The model parameter σ is referred to as the migration ratio and expresses the relative preference of tumor cell migration in white matter over gray matter along the dominant diffusion direction. Studies on mathematical tumor growth models generally use a value between 2 and 100, with a value of 10 commonly used, e.g. [28–30].

Fig. 1 illustrates the effect of choosing different values of σ on the resulting 3D distance map solved with the Hamilton Fast Marching python library [31]. Setting $\sigma = 10$ produces a distance map with highly anisotropic iso-distance contours compared to $\sigma = 1$.

Once the 3D distance map is computed for each patient, the aniso tropic CTV is defined by selecting the level set within the distance map that encompasses the same volume as the CTV used for clinical treatment (15 mm isotropic expansion from GTV). This level set is then extracted and used to define the anisotropic CTV boundary.

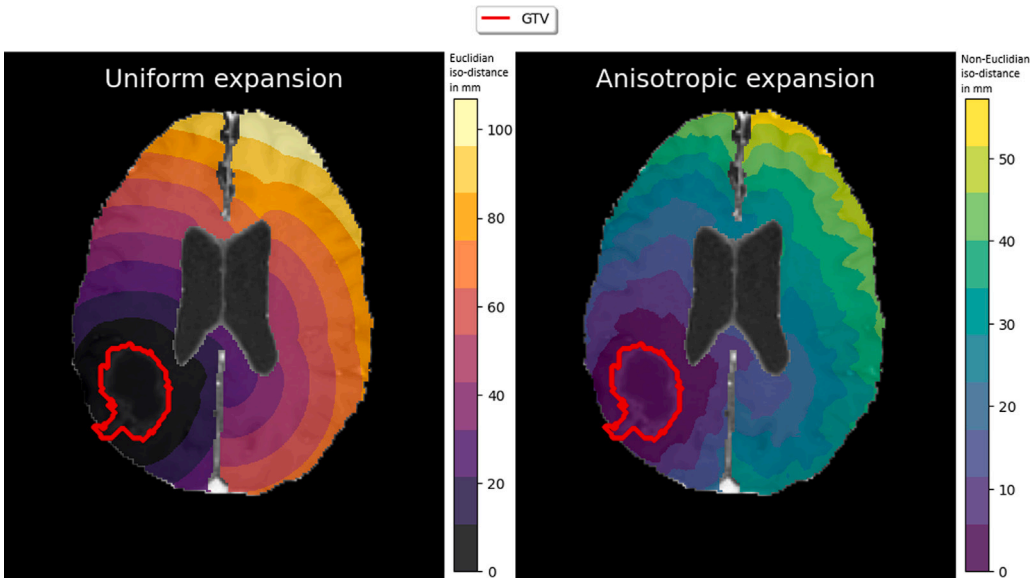

Fig. 1. Example of distance maps using a uniform expansion (left) and anisotropic expansion (right).
3D distance maps calculated with Eq. (1), using different choices of parameter σ in Eq. (3). A value of σ = 1 results in quasi isotropic iso-distance contours (left), while setting and σ = 10 in white matter voxels results in anisotropic iso-distance contours (right). Expansions were restricted by a barrier segmentation, which prevented migration across structures such as the falx cerebri and into the ventricles. Note that the colorbar units in each image are in mm. However, the distance metric used in the anisotropic expansion on the right operates in a non-Euclidean space, where anisotropic regions are effectively "shortened". As a result, the iso-distance contours do not correspond to actual physical distances. GTV: Gross Tumor Volume. mm: millimeters.

2.3. Evaluation of CTV expansions

To evaluate similarity of CTVs we used the Dice Similarity Coefficient (DSC) and 95% percentile Hausdorff distance (HD95). In the following all comparisons were done for migration ratios σ equal to 1, 2, 5, 10, 50 and 100.

We first investigated the feasibility of using an atlas-DTI for aniso tropic CTV expansion, as opposed to a patient-DTI. We did this by comparing the CTVs produced using each of the three atlas and compare them with the CTV produced using the patient-DTI.

Second, we investigated the similarity of the anisotropic CTV expansion to the clinically used CTV, hereafter referred to as *clinical-CTV*. We did this by comparing the surface shape of the anisotropic CTVs produced by the three atlas- and the patient-DTI, to the clinical-CTVs.

2.4. Data pre-processing

Initially all CT images were rigidly registered to T1C, along with GTV, CTV and brain delineations. Linear interpolation was used for images and nearest neighbor for masks. All T1C images underwent skullstripping. If a T1 atlas did not have a skullstripped version available, the Brain Extraction Tool (FSL, version 6.0) [32] was used to extract the brain. Subsequently both patient and atlas images underwent white matter normalization [33] and was rigidly registered into the MNI152 non-linear 6th generation standard-space [34]. Following next, each of the atlas T1 images were deformably registered onto the standardized patient images. The same transformation was then applied to the atlas-DTI, followed by the PPD algorithm.[1] Subsequently, atlas- and patient-DTI with negative eigenvalues were replaced by 1e-14 and all-zero eigenvalues were replaced by the globally smallest non-zero eigenvalue.

White matter and tumor barrier segmentation were computed using Freesurfer [35] version 7.2.0, applying the Sequence Adaptive Multimodal SEGmentation (SAMSEG) [36] functionality. The barrier structures were created by combining the ventricle system, brainstem, cerebellum and Cerebrospinal Fluid (CSF). The CSF segmentation underwent post-processing to resemble falx cerebri and tentorium cerebelli. Subsequently, barrier structures were generated on an independent dataset of GBM patients and a deep learning segmentation model was trained to generate smooth barrier structures with no leaks due to missing voxels in the segmentation. The white matter and barrier segmentations were corrected for faulty segmentations inside the GTV.

2.5. Statistics and software

Pre-processing and estimating of DTI was done using MRtrix3 (version 3.0.3) [37]. Python (version 3.7.12) was used to generate CTV expansions and calculate metrics (packages: AGD-0.2.4, HFM-0.2.12, Nibabel-4.0.2, Tensorflow-2.11.0, Medpy-0.4.0, Surface distance-0.1). 95% Confidence Intervals (CI) were estimated with percentile bootstrapping in 1000 iterations. Significance testing was done using Wilcoxon signed rank test with Holm-Bonferroni correction, using a significance level of 0.01. All statistical analysis was performed in R (version 4.4.0).

3. Results

The results from the use of a warped atlas-DTI are presented below. Figs. 3,4, Table 1, and Supplementary Table 2 show the volumetric and surface similarities of the anisotropic CTVs across all investigated migration ratios. Sections 3.1 and 3.2 focus on a migration ratio of 10 for clarity, as it is the most common value.

3.1. Atlas- versus patient-DTI for anisotropic CTV generation

Evaluating the anisotropic CTVs produced using the three atlas-DTI: HCP, IIT and MIITRA with the volume produced using the patient-DTI, there was no statistically significant difference in DSC between any of the atlas-DTI used: Median (range) were 0.96 (0.93-0.97), 0.96 (0.93-0.97) and 0.95 (0.93-0.97) respectively. The DSC decreased gradually as the migration ratio increased, however the non-significant relation between the CTVs remained. Results were consistent across all metrics (Fig. 2, Fig. 3, Table 1).

[1] https://github.com/ANTsX/ANTs/wiki/Warp-and-reorient-a-diffusion-tensor-image

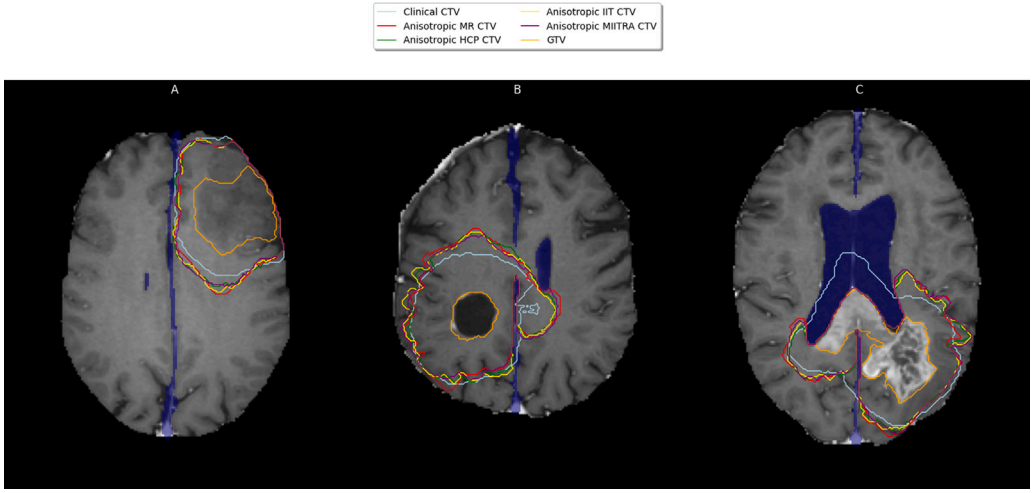

Fig. 2. Three examples of patients with all four anisotropic CTVs and the clinical-CTV.
The three patients differ by their location of the GTV, extent of resection and contrast enhancement. The anisotropic CTVs are generated with a migration ratio equal to 10. Barrier structure is shown in blue. A: Non-contarst enhancing tumor in the right frontal region distant from corpus callosum B: Resection cavity near splenium corporis callosi. Example of minor barrier violations by the clinical-CTV. C: Irregularly shaped contrast enahncing tumor growing through splenium corporis callosi. Instance of substantial barrier violations by the clinical-CTV. GTV: Gross Tumor Volume, CTV: Clinical Tumor Volume, HCP: Human Connectome Project, IIT: Illinois Institute of Technology, MIITRA: Multichannel Illinois Institute of Technology & Rush university Aging.

Table 1
Results from comparing CTVs generated using Atlas-DTI with CTVs generated using Patient-DTI.
DSC: Dice Similarity Coefficient, DTI: Diffusion Tensor Imaging, CTV: Clinical Target Volume, HCP: Human Connectome Project, IIT: Illinois Institute of Technology, MIITRA: Multichannel Illinois Institute of Technology & Rush university Aging, MR: Magnetic Resonance.

Migration.Ratio	Atlas	DSC	HD95	sDSC_1mm
1	HCP	1.00 (1.00, 1.00)	0.0 (0.0, 0.0)	1.00 (1.00, 1.00)
1	IIT	1.00 (1.00, 1.00)	0.0 (0.0, 0.0)	1.00 (1.00, 1.00)
1	MIITRA	1.00 (1.00, 1.00)	0.0 (0.0, 0.0)	1.00 (1.00, 1.00)
2	HCP	0.99 (0.98, 0.99)	1.0 (1.0, 1.4)	0.99 (0.97, 1.00)
2	IIT	0.99 (0.98, 0.99)	1.0 (1.0, 1.4)	0.99 (0.97, 1.00)
2	MIITRA	0.99 (0.98, 0.99)	1.0 (1.0, 1.4)	0.99 (0.96, 1.00)
5	HCP	0.97 (0.95, 0.98)	2.0 (1.0, 2.2)	0.90 (0.83, 0.98)
5	IIT	0.97 (0.95, 0.98)	2.0 (1.4, 2.4)	0.91 (0.83, 0.96)
5	MIITRA	0.97 (0.95, 0.98)	2.0 (1.0, 2.4)	0.90 (0.83, 0.99)
10	HCP	0.96 (0.93, 0.97)	2.3 (1.4, 3.0)	0.86 (0.76, 0.95)
10	IIT	0.96 (0.93, 0.97)	2.4 (1.7, 3.2)	0.86 (0.73, 0.93)
10	MIITRA	0.95 (0.93, 0.97)	2.3 (1.4, 3.0)	0.85 (0.78, 0.96)
50	HCP	0.93 (0.88, 0.96)	2.6 (1.7, 4.5)	0.84 (0.73, 0.94)
50	IIT	0.93 (0.87, 0.96)	2.8 (1.7, 5.1)	0.84 (0.68, 0.94)
50	MIITRA	0.93 (0.86, 0.96)	2.9 (2.2, 5.1)	0.83 (0.67, 0.89)
100	HCP	0.92 (0.86, 0.96)	2.6 (1.4, 5.0)	0.86 (0.76, 0.95)
100	IIT	0.92 (0.83, 0.96)	2.4 (1.4, 5.4)	0.86 (0.70, 0.95)
100	MIITRA	0.92 (0.83, 0.95)	2.6 (1.7, 5.4)	0.85 (0.69, 0.93)

3.2. Anisotropic versus clinical-CTV

When evaluating the anisotropic CTVs generated using each of the DTI sources (HCP, IIT, MIITRA, MR) with the clinical-CTV, we found no statistically significant difference in DSC, between the MR-based CTV and any of the Atlas-based CTVs; 0.87 (0.76-0.92), 0.86 (0.76-0.91), 0.87 (0.76-0.92) and 0.86 (0.76-0.91). Again, DSC decreased as the migration ratio increased and the non-significant relation remained intact. Results were consistent across all metrics (Fig. 4, Supplementary Table 2).

3.3. Influence of migration ratio on similarity between anisotropic- and clinical-CTV

The bootstrapped uncertainty of the median DSC between aniso tropic CTVs made using patient-DTI and clinical-CTV was calculated to be: Median (CI) 0.95 (0.93, 0.96), 0.94 (0.93, 0.95), 0.90 (0.89, 0.91), 0.86 (0.85, 0.88), 0.78 (0.76, 0.80) and 0.73 (0.71, 0.76) for migration ratios 1, 2, 5, 10, 100 respectively. Comparing the CIs across migration ratios, there is an overlap between 1 and 2 as well as 50 and 100 (Supplementary Table 3, Fig. 5). Given that no overlap is considered a distinctive difference, increasing the migration ratio above 2 results in distinctively different anisotropic CTVs compared to the clinical-CTVs.

4. Discussion

We conducted the first head-to-head comparison of multiple atlas-DTI with patient-DTI, for the purpose of developing anisotropic CTVs. Our results show that there was no significant difference between the three atlases when compared to the patient-DTI. In addition, under certain choices of the migration ratio parameter, the anisotropic CTVs could be significantly different from the clinical-CTV. However, each respective difference was statistically insignificant, indicating an equivalence between the use of each DTI source.

Similarly to our study, Stretton et al. [17] reported a non-significant difference between patient- and atlas-DTI for predicting the shape of the tumor infiltration boundary. However, the results were based on only 3 patients (2 low grade gliomas and 1 high grade glioma), which does not encapsulate heterogeneity of the patient group. In addition, patient data included only preoperative patient cases. Surgical intervention may cause disruption of white matter bundles surrounding the resection cavity. Therefore, our study provides a more comprehensive validation of the use of atlas-DTI at the radiation treatment planning stage.

The uncertainties introduced by substituting a patient-DTI with an atlas-DTI can be considered small compared to other sources of uncertainty in the CTV delineation process. For instance, Wee et al. conducted an inter-observer variation study on CTV delineation for GBM. They reported a mean DSC (range) of 0.78 (0.69-0.86) between a calculated consensus- and an expert-contour delineated by a panel of

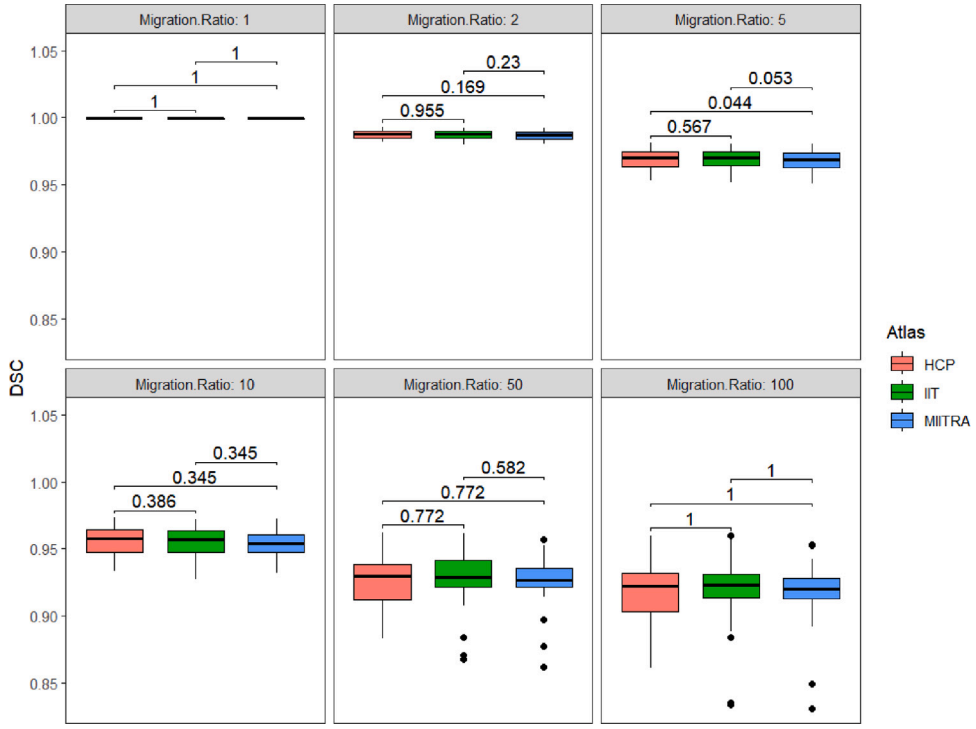

Fig. 3. Feasibility of using an atlas-DTI in place of a patient-DTI.
Comparison of DSC between anisotropic CTVs using Atlas- and Patient-DTI across migrations ratios (1, 2, 5, 10, 50, 100) and atlas versions (HCP, IIT, MIITRA). The p-values for difference comparisons are shown above. DSC: Dice Similarity Coefficient, DTI: Diffusion Tensor Imaging, HCP: Human Connectome Project, IIT: Illinois Institute of Technology, MIITRA: Multichannel Illinois Institute of Technology & Rush university Aging.

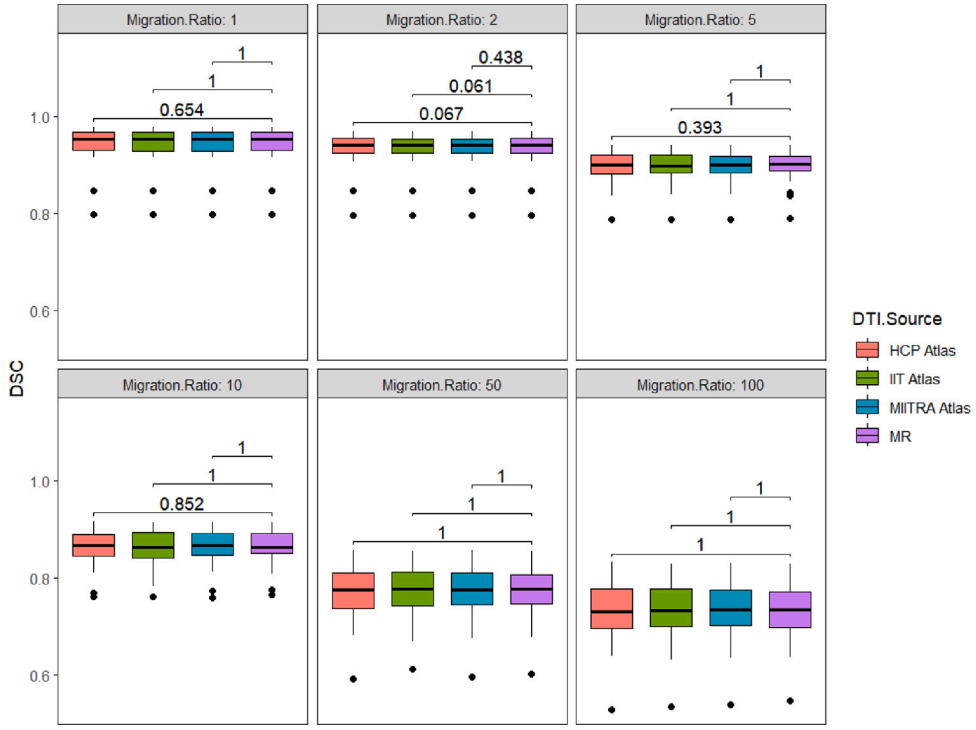

Fig. 4. Similarity of the anisotropic CTVs and the clinical-CTV.
Comparison of DSC between anisotropic CTVs and clinical CTV across migrations ratios (1, 2, 5, 10, 50, 100) and DTI sources (HCP, IIT, MIITRA, MR). The p-values for difference comparisons are show above. DSC: Dice Similarity Coefficient, DTI: Diffusion Tensor Imaging, HCP: Human Connectome Project, IIT: Illinois Institute of Technology, MIITRA: Multichannel Illinois Institute of Technology & Rush university Aging, MR: Magnetic Resonance.

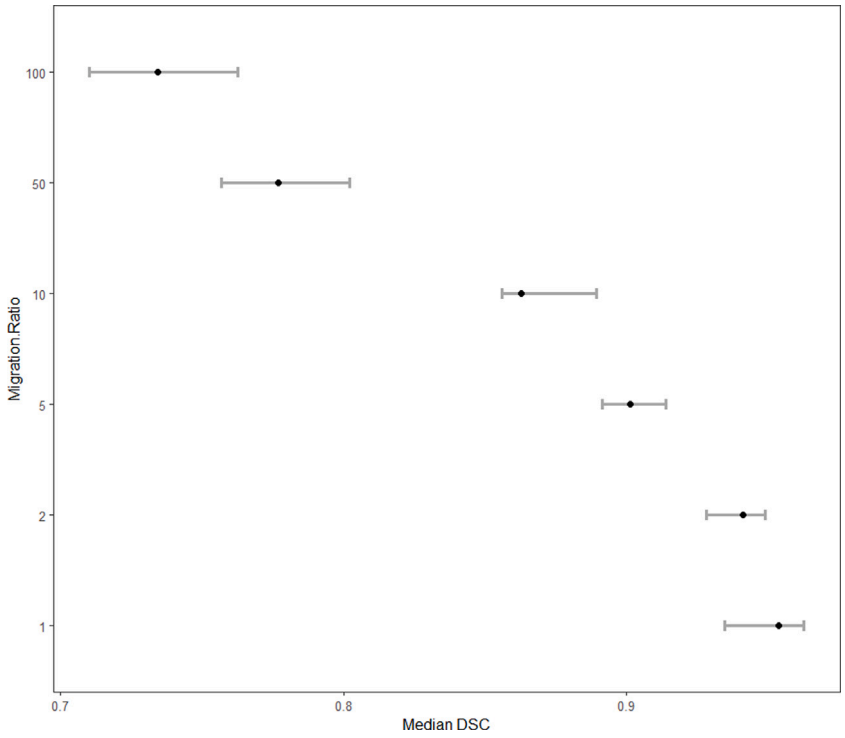

Fig. 5. The influence of migration ratio on similarity between anisotropic CTV and the clinical-CTV.
Bootstrap uncertainty of median DSC on comparison of MR anisotropic CTVs versus clinical-CTVs, across migrations ratios (1, 2, 5, 10, 50, 100). DSC: Dice Similarity Coefficient, MR: Magnetic Resonance, CTV: Clinical Target Volume.

15 radiation oncologists following European guidelines [38]. Although a direct comparison with Wee et al. is not possible due to differing sources of uncertainty, the error introduced by replacing a patient-specific DTI with an atlas-DTI is small compared to other uncertainties in the CTV delineation process. Interestingly, this suggests that an approximate template of brain tissue microstructure is sufficient for predicting tumor infiltration patterns, and any discrepancies between atlas- and patient-DTI have little to no effect. This observation is consistent for all three atlases considered, despite the differences of developmental cohorts in size and age.

Our model converges to the clinical-CTV by choosing a migration ratio equal to 1 under the condition that there are no anatomical barriers in close proximity to the GTV. However, across all DTI sources, the DSC values range from 0.81 to 0.98. In some cases, the clinical-CTV overlapped with barriers, such as the ventricles as shown in Fig. 2. In some patients, the CTV may deviate from the guidelines due to clinical considerations. This places an upper limit on how close an automated model-based CTV can be to the clinical-CTV. In addition, for a given patient, the anisotropic CTV boundary was selected to be the same volumetric size as the clinical CTV. Therefore, any overlap between the clinical-CTV and a barrier structure will result in redistribution of the corresponding anisotropic CTV to other tissues in the brain.

A direct comparison of migration ratios has not previously been explored. The migration ratio determines the extent to which the anisotropic CTV will deviate from the clinical-CTV, but it has no know biological correlate. The precise threshold at which this deviation becomes significant is unclear. To give a guideline for relevant migration ratios that generate substantially different CTVs, we calculated bootstrap uncertainties on the median of the MR-based anisotropic CTVs. The anisotropic CTV with a migration ratio of 1 serves as a reference point for the reproducibility of the clinical-CTV, using the automated method proposed in section 2.2. Our findings show that a migration ratio of 10 is a conservative choice that results in a substantially different CTV, while still retaining a large portion of the original CTV. Interestingly, migration ratios of 50 and 100 provide somewhat similar volumes. This is most likely due to the volumetric size restriction defined by the clinical-CTV. As the migration ratio increases, the expansion model shifts volume from gray matter into white matter. However, because the amount of gray matter is limited, this migration diminishes at higher migration ratios, resulting in similar volumes. Therefore, the range of relevant migration ratios in our dataset is limited to between 5 and 50.

We identified the following limitations for this study. Using DTI data for estimating anisotropic CTV margins requires the transformation of diffusion tensors to metric tensors for inclusion in the shortest path algorithm. We can only determine this transformation up to a constant [26]. This is a single center study and difference in DTI scan sequences and MRI scanners could potentially have an influence. We did not attempt to determine whether the differences between atlas- and patient-DTI based CTVs were caused by microstructural breakdowns in the white matter tracts due to tumor infiltration or by inconsistencies between atlas- and patient-DTI. Having this information available would provide a clearer understanding of the potential improvements.

GBM is a challenging tumor to treat, and understanding its infiltration and recurrence patterns is crucial for developing more personalized treatment strategies. Recent studies have explored the potential to predict GBM infiltration in the peritumoral region, with promising results [39–42]. This research could potentially support the use of an anisotropic CTV by identifying high- and low-risk regions, offering guidance for selecting a patient-specific migration ratio that effectively covers high-risk areas while sparing low-risk ones. In our study, the anisotropic CTV is constrained by the volume of the clinical CTV. However, with information about high-risk areas available, an oncologist may choose to extend beyond these constraints, allowing for a larger anisotropic CTV than would typically be accepted with a standard 15 mm isotropic expansion. Conversely, a more flexible CTV definition could also enable an overall reduced volume while maintaining similar recurrence coverage, to the current standard.

Currently, DTI plays little to no role in clinical practice of radiotherapy treatment planning for glioblastoma due to a lack of supporting

evidence. Our study demonstrates that using an atlas-DTI is a viable alternative to a patient-DTI. This approach enables retrospective studies of anisotropic CTVs across large cohorts, which could provide the necessary evidence to support its integration into clinical practice. Furthermore, the atlas-DTI method has the potential to render patient-specific DTI unnecessary for anisotropic CTV generation.

Our results show that the use of atlas DTI produces very similar anisotropic CTV volumes compared to patient DTI. This suggests that the use of atlas-DTI for the purpose of anisotropic CTV expansion is a viable alternative to patient DTI.

CRediT authorship contribution statement

Kim Hochreuter: Methodology, Investigation, Data curation, Conceptualization, Formal analysis, Writing – original draft, Visualization . **Gregory Buti:** Methodology, Validation, Software, Writing – original draft, Writing – review & editing. **Ali Ajdari:** Writing – review & editing. **Christopher P. Bridge:** Writing – review & editing. **Gregory C. Sharp:** Writing – review & editing. **Slávka Lukacova:** Resources, Writing – review & editing. **Thomas Bortfeld:** Methodology, Conceptualization, Writing – review & editing, Supervision. **Jesper F. Kallehauge:** Methodology, Conceptualization, Writing – review & editing, Supervision, Funding acquisition.

Funding

This work was supported by the Danish Cancer Society (grant no. R302-A17263) and the Danish Comprehensive Cancer Center - Brain Tumor Center (grant no. R302-A17263-B392 & R295-A16770).

Declaration of competing interest

The authors declare that they have no known competing financial interests or personal relationships that could have appeared to influence the work reported in this paper.

Appendix A. Supplementary data

Supplementary material related to this article can be found online at https://doi.org/10.1016/j.phro.2024.100688.

References

[1] Stupp R, Mason WP, van den Bent MJ, Weller M, Fisher B, Taphoorn MJ, et al. Radiotherapy plus concomitant and adjuvant temozolomide for glioblastoma. N Engl J Med 2005;352(10):987–96. http://dx.doi.org/10.1056/NEJMoa043330, PMID: 15758009.

[2] Niyazi M, Andratschke N, Bendszus M, Chalmers AJ, Erridge SC, Galldiks N, et al. ESTRO-EANO guideline on target delineation and radiotherapy details for glioblastoma. Radiother Oncol 2023;184:109663. http://dx.doi.org/10.1016/j.radonc.2023.109663.

[3] Halperin EC, Bentel G, Heinz E, Burger PC. Radiation therapy treatment planning in supratentorial glioblastoma multiforme: An analysis based on post mortem topographic anatomy with ct correlations. Int J Radiat Oncol*Biol*Phys 1989;17(6):1347–50. http://dx.doi.org/10.1016/0360-3016(89)90548-8.

[4] Watanabe M, Tanaka R, Takeda N. Magnetic resonance imaging and histopathology of cerebral gliomas. Neuroradiology 1992;34(6):463–9. http://dx.doi.org/10.1007/bf00598951.

[5] Johnson PC, Hunt SJ, Drayer BP. Human cerebral gliomas: correlation of postmortem MR imaging and neuropathologic findings. Radiology 1989;170(1):211–7. http://dx.doi.org/10.1148/radiology.170.1.2535765.

[6] Kelly PJ, Daumas-Duport C, Kispert DB, Kall BA, Scheithauer BW, Illig JJ. Imaging-based stereotaxic serial biopsies in untreated intracranial glial neoplasms. J Neurosurg 1987;66(6):865–74. http://dx.doi.org/10.3171/jns.1987.66.6.0865.

[7] Price SJ, Jena R, Burnet NG, Hutchinson PJ, Dean AF, a A, et al. Improved delineation of glioma margins and regions of infiltration with the use of diffusion tensor imaging: an image-guided biopsy study. AJNR Am J Neuroradiol 2006;27(9):1969–74.

[8] Soares JM, Marques P, Alves V, Sousa N. A hitchhiker's guide to diffusion tensor imaging. Front Neurosci 2013;7:31.

[9] Tae WS, Ham BJ, Pyun SB, Kang SH, Kim BJ. Current clinical applications of diffusion-tensor imaging in neurological disorders. J Clin Neurol 2018;14(2):129–40.

[10] O'Donnell LJ, Westin CF. An introduction to diffusion tensor image analysis. Neurosurg Clin N Am 2011;22(2). 185–96, viii.

[11] Jbabdi S, Mandonnet E, Duffau H, Capelle L, Swanson KR, Pélégrini-Issac M, et al. Simulation of anisotropic growth of low-grade gliomas using diffusion tensor imaging. Magn Reson Med 2005;54(3):616–24. http://dx.doi.org/10.1002/mrm.20625.

[12] Konukoglu E, Clatz O, Menze B, Stieltjes B, Weber MA, Mandonnet E, et al. Image guided personalization of reaction-diffusion type tumor growth models using modified anisotropic eikonal equations. IEEE Trans Med Imaging 2010;29(1):77–95. http://dx.doi.org/10.1109/tmi.2009.2026413.

[13] Unkelbach J, Menze BH, Konukoglu E, Dittmann F, Ayache N, Shih HA. Radiotherapy planning for glioblastoma based on a tumor growth model: implications for spatial dose redistribution. Phys Med Biol 2014;59(3):771, Available from:c.

[14] Yuan J, Liu L. Brain glioma growth model using reaction-diffusion equation with viscous stress tensor on brain MR images. Magn Reson Imaging 2016;34(2):114–9. http://dx.doi.org/10.1016/j.mri.2015.10.012.

[15] Jensen MB, Guldberg TL, Harbøll A, Lukacova S, Kallehauge JF. Diffusion tensor magnetic resonance imaging driven growth modeling for radiotherapy target definition in glioblastoma. Acta Oncol 2017;56(11):1639–43. http://dx.doi.org/10.1080/0284186x.2017.1374559.

[16] Buti G, Ajdari A, Hochreuter K, Shih H, Bridge CP, Sharp GC, et al. The influence of anisotropy on the clinical target volume of brain tumor patients. Phys Med Biol 2024;69(3):035006. http://dx.doi.org/10.1088/1361-6560/ad1997.

[17] Stretton E, Geremia E, Menze B, Delingette H, Ayache N. Importance of patient DTI's to accurately model glioma growth using the reaction diffusion equation. In: 2013 IEEE 10th international symposium on biomedical imaging. IEEE; 2013.

[18] Wesseling P, Capper D. WHO 2016 classification of gliomas. Neuropathol Appl Neurobiol 2018;44(2):139–50.

[19] Tahedl M. B.A.T.M.A.N.: Basic and advanced tractography with mrtrix for all neurophiles. 2022, http://dx.doi.org/10.17605/OSF.IO/FKYHT, Available from: https://osf.io/fkyht/.

[20] Ades-Aron B, Veraart J, Kochunov P, McGuire S, Sherman P, Kellner E, et al. Evaluation of the accuracy and precision of the diffusion parameter estimation with gibbs and noise removal pipeline. Neuroimage 2018;183:532–43. http://dx.doi.org/10.1016/j.neuroimage.2018.07.066, Available from: https://www.sciencedirect.com/science/article/pii/S1053811918306827.

[21] Glasser MF, Sotiropoulos SN, Wilson JA, Coalson TS, Fischl B, Andersson JL, et al. The minimal preprocessing pipelines for the human connectome project. Neuroimage 2013;80:105–24.

[22] Zhang S, Arfanakis K. Evaluation of standardized and study-specific diffusion tensor imaging templates of the adult human brain: Template characteristics, spatial normalization accuracy, and detection of small inter-group FA differences. Neuroimage 2018;172:40–50.

[23] Wu Y, Ridwan AR, Niaz MR, Qi X, Zhang S, Alzheimer's Disease Neuroimaging Initiative, et al. Development of high quality T1-weighted and diffusion tensor templates of the older adult brain in a common space. Neuroimage 2022;260:119417. http://dx.doi.org/10.1016/j.neuroimage.2022.119417, Available from: https://www.sciencedirect.com/science/article/pii/S1053811922005341.

[24] Avants BB, Tustison NJ, Song G, Cook PA, Klein A, Gee JC. A reproducible evaluation of ANTs similarity metric performance in brain image registration. Neuroimage 2011;54(3):2033–44.

[25] Alexander D, Pierpaoli C, Basser P, Gee J. Spatial transformations of diffusion tensor magnetic resonance images. IEEE Trans Med Imaging 2001;20(11):1131–9. http://dx.doi.org/10.1109/42.963816.

[26] Bortfeld T, Buti G. Modeling the propagation of tumor fronts with shortest path and diffusion models—implications for the definition of the clinical target volume. Phys Med Biol 2022;67(15):155014. http://dx.doi.org/10.1088/1361-6560/ac8043.

[27] Niethammer M, Estepar RSJ, Bouix S, Shenton M, Westin CF. On diffusion tensor estimation. In: 2006 international conference of the IEEE engineering in medicine and biology society. IEEE; 2006.

[28] Lipkova J, Angelikopoulos P, Wu S, Alberts E, Wiestler B, Diehl C, et al. Personalized radiotherapy design for glioblastoma: Integrating mathematical tumor models, multimodal scans, and Bayesian inference. IEEE Trans Med Imaging 2019;38(8):1875–84. http://dx.doi.org/10.1109/tmi.2019.2902044.

[29] Lipkova J, Chen RJ, Chen B, Lu MY, Barbieri M, Shao D, et al. Artificial intelligence for multimodal data integration in oncology. Cancer Cell 2022;40(10):1095–110.

[30] Martens C, Rovai A, Bonatto D, Metens T, Debeir O, Decaestecker C, et al. Deep learning for reaction-diffusion glioma growth modeling: Towards a fully personalized model? Cancers 2022;14(10):2530. http://dx.doi.org/10.3390/cancers14102530.

[31] Mirebeau JM, Portegies J. Hamiltonian Fast Marching: A Numerical Solver for Anisotropic and Non-Holonomic Eikonal PDEs. Image Process Line 2019;9:47–93. http://dx.doi.org/10.5201/ipol.2019.227.

[32] Jenkinson M, Beckmann CF, Behrens TEJ, Woolrich MW, Smith SM. FSL. Neuroimage 2012;62(2):782–90.

[33] Reinhold JC, Dewey BE, Carass A, Prince JL. Evaluating the impact of intensity normalization on MR image synthesis. In: Angelini ED, Landman BA, editors. Medical imaging 2019: image processing. SPIE; 2019.

[34] Grabner G, Janke AL, Budge MM, Smith D, Pruessner J, Collins DL. Symmetric atlasing and model based segmentation: An application to the hippocampus in older adults. In: Larsen R, Nielsen M, Sporring J, editors. Medical image computing and computer-assisted intervention – MICCAI 2006. Berlin, Heidelberg: Springer; 2006, p. 58–66.

[35] Fischl B. FreeSurfer. Neuroimage 2012;62(2):774–81.

[36] Puonti O, Iglesias JE, Van Leemput K. Fast and sequence-adaptive whole-brain segmentation using parametric Bayesian modeling. Neuroimage 2016;143:235–49.

[37] Tournier JD, Smith R, Raffelt D, Tabbara R, Dhollander T, Pietsch M, et al. MRtrix3: A fast, flexible and open software framework for medical image processing and visualisation. Neuroimage 2019;202:116137. http://dx.doi.org/10.1016/j.neuroimage.2019.116137.

[38] Wee CW, Sung W, Kang HC, Cho KH, Han TJ, Jeong BK, et al. Evaluation of variability in target volume delineation for newly diagnosed glioblastoma: a multi-institutional study from the Korean radiation oncology group. Radiat Oncol 2015;10(1). http://dx.doi.org/10.1186/s13014-015-0439-z.

[39] Rathore S, Akbari H, Doshi J, Shukla G, Rozycki M, Bilello M, et al. Radiomic signature of infiltration in peritumoral edema predicts subsequent recurrence in glioblastoma: implications for personalized radiotherapy planning. J Med Imaging (Bellingham) 2018;5(2):021219.

[40] Cepeda S, Luppino LT, Pérez-Núñez A, Solheim O, García-García S, Velasco-Casares M, et al. Predicting regions of local recurrence in glioblastomas using voxel-based radiomic features of multiparametric postoperative MRI. Cancers (Basel) 2023;15(6).

[41] Kwak S, Akbari H, Garcia JA, Mohan S, Dicker Y, Sako C, et al. Predicting peritumoral glioblastoma infiltration and subsequent recurrence using deep-learning-based analysis of multi-parametric magnetic resonance imaging. J Med Imaging (Bellingham) 2024;11(5):054001.

[42] Xing Z, Wang C, Yang W, She D, Yang X, Cao D. Predicting glioblastoma recurrence using multiparametric MR imaging of non-enhancing peritumoral regions at baseline. Heliyon 2024;10(9):e30411.